Article

SOURCE DATA

THE EMBO JOURNAL

Miro1 regulates intercellular mitochondrial transport & enhances mesenchymal stem cell rescue efficacy

Tanveer Ahmad[1,†], Shravani Mukherjee[1,†], Bijay Pattnaik[1], Manish Kumar[1], Suchita Singh[1], Manish Kumar[2], Rakhshinda Rehman[1], Brijendra K Tiwari[3], Kumar A Jha[4], Amruta P Barhanpurkar[5], Mohan R Wani[5], Soumya S Roy[1], Ulaganathan Mabalirajan[1], Balaram Ghosh[1] & Anurag Agrawal[1,*]

Abstract

There is emerging evidence that stem cells can rejuvenate damaged cells by mitochondrial transfer. Earlier studies show that epithelial mitochondrial dysfunction is critical in asthma pathogenesis. Here we show for the first time that Miro1, a mitochondrial Rho-GTPase, regulates intercellular mitochondrial movement from mesenchymal stem cells (MSC) to epithelial cells (EC). We demonstrate that overexpression of Miro1 in MSC (MSCmiro^{Hi}) leads to enhanced mitochondrial transfer and rescue of epithelial injury, while Miro1 knockdown (MSCmiro^{Lo}) leads to loss of efficacy. Treatment with MSCmiro^{Hi} was associated with greater therapeutic efficacy, when compared to control MSC, in mouse models of rotenone (Rot) induced airway injury and allergic airway inflammation (AAI). Notably, airway hyperresponsiveness and remodeling were reversed by MSCmiro^{Hi} in three separate allergen-induced asthma models. In a human *in vitro* system, MSCmiro^{Hi} reversed mitochondrial dysfunction in bronchial epithelial cells treated with pro-inflammatory supernatant of IL-13-induced macrophages. Anti-inflammatory MSC products like NO, TGF-β, IL-10 and PGE2, were unchanged by Miro1 overexpression, excluding non-specific paracrine effects. In summary, Miro1 overexpression leads to increased stem cell repair.

Keywords asthma; mesenchymal stem cells; Miro1/Rhot1; mitochondria; nanotubes

Subject Categories Membrane & Intracellular Transport; Stem Cells

DOI 10.1002/embj.201386030 | Received 19 June 2013 | Revised 3 December 2013 | Accepted 5 December 2013 | Published online 15 January 2014

The EMBO Journal (2014) 33: 994–1010

See also: **G Las & OS Shirihai *et al*** (May 2014)

Introduction

Mitochondria, the powerhouse of cells, are important regulators of cell survival and cell death (Liesa *et al*, 2009; Youle & van der Bliek, 2012), particularly via release of reactive oxygen species (ROS) and activation of apoptotic pathways (Johnson *et al*, 1996; Galluzzi *et al*, 2012). Mitochondrial damage is seen in a wide variety of pathological conditions, including inflammation (Gomes *et al*, 2011). Since the first report of mitochondrial transfer from human stem cells (Spees *et al*, 2006), there has been an interest in testing this mechanism for exogenous replacement of damaged mitochondria, thereby rescuing cells from death (Yasuda *et al*, 2011; Cho *et al*, 2012). The efforts have been complicated by limited knowledge regarding the mechanisms of inter-cellular mitochondrial transfer (Prockop, 2012). It is already known that intracellular mitochondrial movement is mediated by regulated mitochondrial transport machinery (Quintero *et al*, 2009; Brickley & Stephenson, 2011; Chang *et al*, 2011). In extensive studies in neuronal cells, Miro1 (mitochondrial Rho GTPase 1, synonym: Rhot1), a calcium-sensitive adaptor protein that attaches the mitochondria to the KIF5 motor proteins, with the help of a set of accessory proteins like Miro2, TRAK1, TRAK2 and Myo19, aids the mitochondria to move along microtubules inside the cells (Quintero *et al*, 2009; Brickley & Stephenson, 2011; Chang *et al*, 2011). Inhibiting the attachment of mitochondria on microtubules and consequently restricting its movement, by Miro1 inhibition, offers an attractive tool for dissection of mitochondrial donation.

A recent work showed that in a mouse model of induced acute lung injury, exogenous intra-tracheal administration of mesenchymal stem cells (MSC) was associated with mitochondrial donation to alveolar epithelial cells, improving their bioenergetic profile and ameliorating the lung injury (Islam *et al*, 2012). While it was shown that MSC with either inability to form gap junctions or with

1 Centre of Excellence in Asthma & Lung Disease, CSIR-Institute of Genomics and Integrative Biology, Delhi, India
2 Central Instrumentation Facility, Biotech Centre, University of Delhi South Campus, Delhi, India
3 Department of Allergy and Infectious Diseases, CSIR-Institute of Genomics and Integrative Biology, Delhi, India
4 Department of Anatomy, All India Institute of Medical Sciences, Delhi, India
5 Department of Cell Biology, National Centre for Cell Science, Pune University Campus, Pune, India
*Corresponding author. Tel: 011 27662075; Fax: 011 27667471; E-mail: a.agrawal@igib.res.in
†These authors contributed equally to this work.

defective mitochondria were ineffective, bioenergetically driven transfer of other organelles via cell-cell connections (Rustom *et al*, 2004) could also be disrupted in the above scenarios. Selective inhibition of mitochondrial transfer would clarify this possibility but requires an understanding of the mitochondrial transfer machinery that regulates intercellular mitochondrial transport (Wang *et al*, 2011). If intercellular mitochondrial donation is an extension of intracellular mitochondrial movement, it appears likely that other mitochondria rich cells could also act as mitochondrial donors. This too has not been investigated.

This subject is extremely relevant to bronchial epithelial injury, a critical aspect of asthma (Ahmad *et al*, 2012), where others and we have previously shown the importance of mitochondrial dysfunction (Mabalirajan *et al*, 2008; Aguilera-Aguirre *et al*, 2009). We investigated the molecular regulation of intercellular mitochondrial transfer and subsequently engineered the donor cells for more effective mitochondrial donation. Bioengineered MSC that overexpress Miro1 had greater mitochondrial donor capacity and were therapeutically more effective in various experimental mouse models of airway injury and asthma, than control MSC.

Results

Mesenchymal cells rescue epithelial cell stress by mitochondrial donation via intercellular tunnelling nanotubes (TNT)

Several previous studies (Rustom *et al*, 2004; Wang *et al*, 2010; Yasuda *et al*, 2011; Islam *et al*, 2012) have shown the possibility of intercellular organelle transport between cells through formation of cytoplasmic bridges termed TNT, which are cytoskeletal-derived structures constituted of actin, as observed with Phalloidin staining. Similarly, we observed the formation of intercellular TNT among lung epithelial cells (EC) like BEAS-2B, LA-4 and NHBE (Supplementary Fig S1A), and were able to visualize mitochondrial movement through these TNT in MSC (Fig 1A; Supplementary Movie S1). The formation of TNT between epithelial cells (EC) or MSC was observed to increase after stress induction by either rotenone (100 nM) or TNF-α (20 ng) (Fig 1B, Supplementary Fig S1B). shRNA-mediated knockdown of TNFAIP2, which is known (Hase *et al*, 2009) to mediate TNT formation, resulted in significant reduction of TNT formation in LA-4 epithelial cells and abrogated mitochondrial transfer (Supplementary Fig S1C). For quantitative assessment of mitochondrial transfer, MSC were transfected with mGFP and co-cultured with EC. After 0 h or 24 h of co-culture, cells were labeled with an epithelial cell-specific marker (EpCAM). EpCAM was used to gate on EC and mitochondrial transfer from MSC to EC was quantified by measuring mGFP counts in EC (Supplementary Fig S1D). Another approach used to quantify the mitochondrial transfer was by separately transfecting MSC and EC with different fluorophores followed by co-culture and imaging or FACS. Typical FACS dot-plots of co-culture experiments are included in Supplementary Datasets 1 and 2. Maximal mitochondrial transfer was seen when EC were stressed (by rotenone) and the MSC were healthy. To determine whether the mitochondrial donor property of MSC was seen in other cells of mesenchymal origin (ME), mouse fibroblasts (3T3) and human smooth muscle cells (SMC) were co-cultured with mouse lung epithelial (LA-4) and human normal bronchial epithelial cells (NHBE), respectively. While mitochondrial transfer from ME to stressed EC was seen (Fig 1D), it was about 70% less than that for MSC under similar conditions (LA-4; Fig 1C and D). Mitochondrial transfer from MSC/ME was increased when EC were treated with mitochondrial specific inhibitors (rotenone, antimycin) or inflammatory stress-inducers (TNF-α and IL-13) (Supplementary Fig S1E and F), while it was reduced when MSC itself was treated with the mitochondrial stress inducer rotenone (Rot) (Fig 1C). While we specifically looked for transfer of mitochondria in the reverse direction i.e. from EC to MSC, this was not observed by either live cell imaging (Supplementary Movie S2), or FACS, even when EC were un-induced and MSC were stress-induced. In our imaging studies, we were able to precisely distinguish MSC, transfected with mRFP, and EC labeled with mGFP, by staining either a MSC surface marker, CD90, or an epithelial cell specific marker, CCSP. We clearly observed mRFP-labeled mitochondria (red), from MSC, inside EC (seen either as red or yellow when donated to EC with mGFP green mitochondria). This is shown for LA-4 mouse lung epithelial cells (Supplementary Movie S2, Fig 1E), and primary mouse tracheal epithelial cells (mTEC) (Fig 1F). Usually, the mitochondrial donation is seen as a few red or yellow mitochondria on the merged images inside some of the green cells, with poorly seen TNT (see Fig 1E and Supplementary Images file in accompanying Dataset 3). The degree and clarity of mitochondrial transfer seen in Fig 1F is less common. Importantly, EC (BEAS-2B and A549) showed no such capacity for mitochondrial transfer among each other (Supplementary Fig S1G). We next determined whether mitochondrial donation was associated with reduction in cell stress. Cell stress was measured in EC by measurement of mitochondrial ROS using mitoSOX red. MSC co-culture markedly attenuated EC cell stress (Fig 1G and H), but ME (Fig 1I) co-culture had a much smaller effect. Co-culture with other EC (Fig 1J) did not show any rescue effect. MSC-mediated EC rescue was lost if MSC were pretreated with rotenone or antimycin (Supplementary Fig S2A), suggesting that functional MSC mitochondria were required for the rescue. Notably, supernatant from cultured MSC did not significantly attenuate mitochondrial ROS, excluding a major role for secreted products (Supplementary Fig S2B). The murine MSC used for all our experiments were characterized by very low expression of CD45 and CD11b and with high expression of Sca-1 (Zhu *et al*, 2010), CD44 and CD105 as analyzed by FACS method (Supplementary Fig S2C). Our experiments were not associated with changes in mitochondrial potential that can confound mitoSOX readings (Supplementary Fig S2D). While we did not directly measure the effects of rotenone and MSC treatments on mitochondrial oxygen consumption, rotenone treatment was associated with an increase in intracellular oxygen concentration in LA-4 epithelial cells, which was almost completely reversed after MSC treatment (Supplementary Fig S2E). This is consistent with reduced mitochondrial oxygen consumption in stressed epithelial cells, which normalizes after MSC-mediated mitochondrial donation.

Thus, MSC can donate mitochondria to stressed EC via cytoplasmic bridges, and attenuate cell stress via mitochondria-dependent mechanism. While other mesenchymal cells can also donate mitochondria, the capacity and the consequent rescue is much lower.

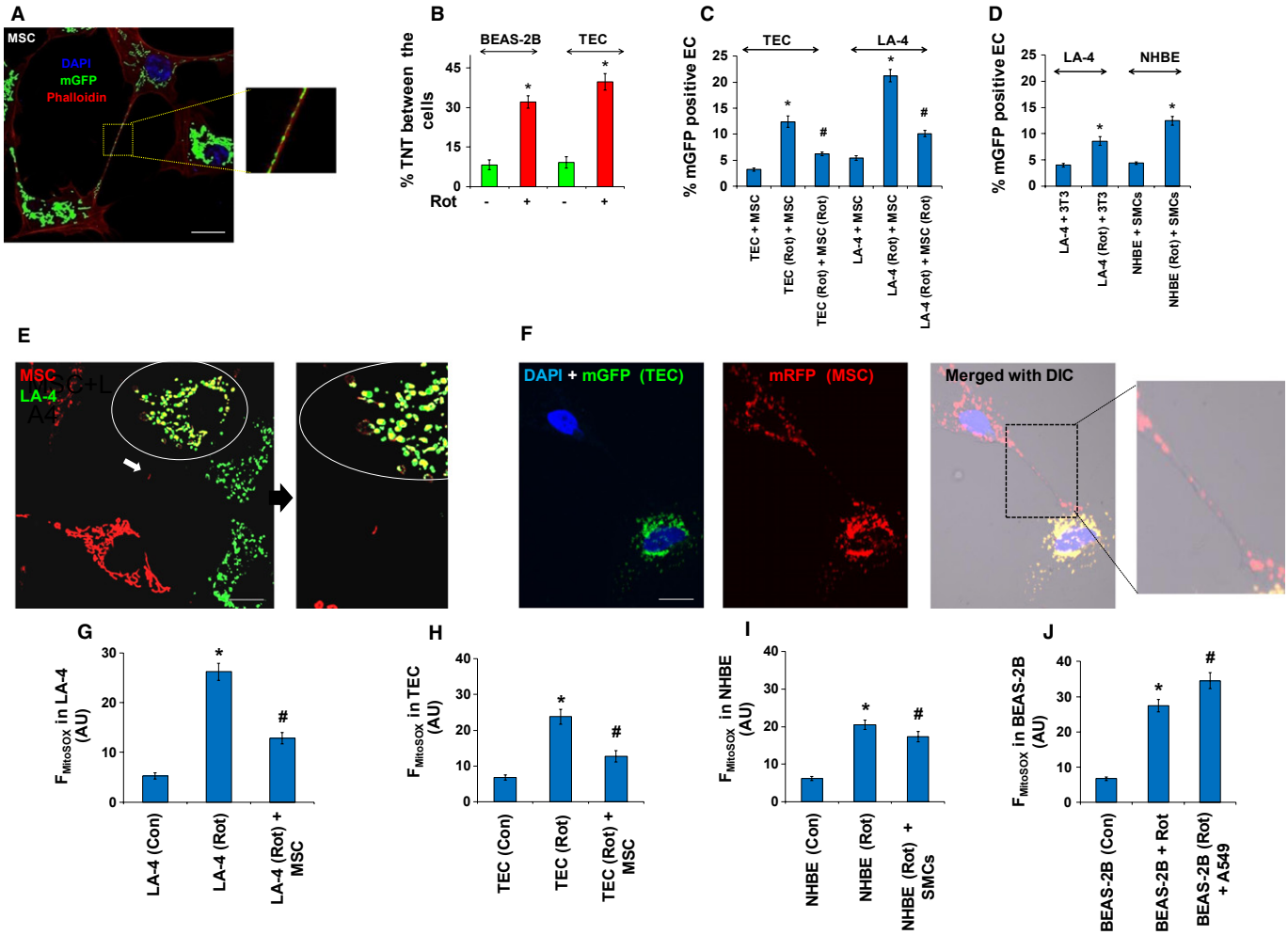

Figure 1. Stem cells show high-efficiency mitochondrial transfer and rescue of stressed airway epithelial cells.

A Representative image of TNT between MSC containing mitochondria labeled with mGFP (green), TNT stained with phalloidin (red) and nuclei with DAPI (blue).

B Increase in TNT formation as quantified among BEAS-2B cells and among mTEC with rotenone induction.

C Quantitative FACS measurement of total percentage of mitochondria in LA-4 or mTEC, which were donated by healthy MSC or rotenone-stressed MSC (MSC (Rot)).

D Quantitative FACS measurement of total percentage of mitochondria, which were donated by 3T3 or SMCs, in rotenone-treated LA-4 or NHBE cells.

E Representative image of mitochondria transferred from mRFP labeled MSC to stress-induced mGFP-labeled LA-4. The encircled enlarged region, indicated by the black arrow, shows accumulation of red mitochondria in one of the green LA-4 cells, seen as yellow or red. The white arrow marks red mitochondria moving from MSC to the LA-4 (confirmed on time lapse images, see accompanying dataset 3).

F Illustrative image of accumulation and migration of mitochondria (mRFP) via nanotubes (enlarged view in inset of "merged with DIC" panel) from MSC into mGFP-labeled stress-induced TEC; nucleus labeled with DAPI.

G–J Total mtROS measured in rotenone-treated LA-4 (G), TEC (H), NHBE (I) and BEAS-2B (J) cells with or without co-culture with MSC, SMCs or A549. Cells were treated with or without rotenone (Rot), and mtROS were measured and expressed as mean fluorescence intensity ($F_{MitoSOX}$) after 24 h of co-culture by gating on epithelial cells (LA-4, TEC, NHBE and BEAS-2B).

Data information: In (A, E and F): scale bar, 10 μm. In (B–D) and (G–J): data are shown as mean ± s.e.m. of three independent experiments, $^{*}P < 0.05$ versus Con and $^{\#}P < 0.05$ versus Rot.

Exogenous administration of stem cells leads to mitochondrial transfer and reverses rotenone-induced airway epithelial injury

In an effort to validate our *in vitro* finding, we developed an *in vivo* mouse model of mitochondrial dysfunction and lung injury by either intra-nasal (i.n.) or intra-tracheal (i.t.) administration of rotenone (Supplementary Movie S3). We initially used different concentrations of rotenone to induce lung injury (Supplementary Fig S3A). Rotenone administration was associated with a significant increase in airway hyperresponsiveness (AHR), cellular infiltration and bronchial epithelial (BE) cell apoptosis (Supplementary Fig S3B–D). Rotenone administration was also associated with a dose-dependent reduction in mitochondrial complex-IV activity, decrease in ATP levels and increase in caspase-3 expression (Supplementary Fig S3E–G) indicating mitochondrial dysfunction associated cell stress. FACS quantification of apoptosis in different lung cells was done, by double

labeling of different lung cell populations specifically CCSP for bronchial epithelial cells (BE), SPC for alveolar epithelial cells (AE), alpha smooth muscle actin (α-SMA) for mesenchymal cells (ME) and F4/80 for macrophages (Ma), along with co-labeling of fluorochrome conjugated apoptotic marker TUNEL. The rotenone dosage of 0.3 mg/kg of body weight was chosen for further experiments, in which, FACS data revealed a predominant bronchial epithelial cell apoptosis followed by AE, ME and Ma (Supplementary Fig S4A). Thus, at this dose of rotenone, airway injury was the most prominent feature with a milder affect on alveolar region. We first determined whether MSC donate mitochondria *in vivo* to injured airway epithelial cells, leading to rescue from cell death. MSC, with mGFP-labeled mitochondria, were intratracheally (i.t.) administered (Supplementary Movie S3) 12 h after rotenone administration, and euthanized 6 and 24 h post MSC treatment. Lungs were dissected and mitochondrial transfer to lung cells was estimated by imaging of cryofrozen section followed by FACS. MSC with mGFP were seen homing the bronchial epithelium at 6 h post treatment (Supplementary Fig S4B) and transfer of mGFP labeled mitochondria from MSC to airway epithelial cells could be seen as punctate green or yellow regions in red $CCSP^{+}$ epithelium (Fig 2A), after 24 h of MSC administration. Quantification of mGFP transfer to $CCSP^{+}$ lung bronchial epithelial cells (BE) was done by FACS (Fig 2B). Rotenone-treated lungs, showed greater mGFP mitochondria transfer to BE cells, analogous to the data in cultured cells (see Fig 1). As seen *in vitro*, rotenone-treated MSC showed decreased mitochondrial transfer from MSC to BE cells (Fig 2B). To estimate mitochondrial transfer to other cell populations in total lung, selective gating of each cell population was performed and mGFP positive fraction was calculated from the FACS data. Mitochondrial donation from MSC to lung increased if lung was induced with rotenone and decreased if MSC were pre-induced with rotenone (Supplementary Fig S4C). The results also revealed that bronchial epithelial cells were the predominant cell types that received mitochondria from the MSC (Fig 2B; Supplementary Fig S4D), followed by alveolar epithelial cells, mesenchymal cells and macrophages. These differences may relate to anatomic or physiological factors, as well as the extent of injury. Mitochondrial donation was associated with reduction of caspase-3 and caspase-9 expression (Supplementary Fig S4E and F) leading to consequent decrease in bronchial epithelial apoptosis (Fig 2C) and inflammation (Fig 2D). This also caused reversal of mitochondrial dysfunction and restoration of bioenergetics, as quantified by increase in ATP levels in the lung (Fig 2E), decrease in cytochrome c in cytosolic extract of lung (Fig 2F), as well as recovery of mitochondrial complex I and IV activities (Fig 2G and H). No therapeutic effects were seen when MSC were pre-induced with rotenone. We also studied self-reversibility of rotenone-induced pathologies over a 7-day period and found that the rotenone-induced lung injury does not spontaneously improve during this period (Supplementary Fig S4G).

These results confirmed that mitochondrial donation from MSC rescue bronchial epithelial cells during mitochondrial dysfunction associated airway injury.

Miro1 is an integral protein involved in mitochondrial transport from MSC to epithelial cells

Other studies (Spees *et al*, 2006; Islam *et al*, 2012) have implied a role of mitochondrial donation-mediated rescue by MSC, but none have elucidated the molecular mechanism involved in intercellular transport of mitochondria from MSC. Since rotenone induction in MSC inhibited mitochondrial donation *in vitro* and *in vivo* (see Figs 1 and 2), we studied the expression pattern of various components of already reported (Quintero *et al*, 2009; Brickley & Stephenson, 2011; Chang *et al*, 2011) intracellular mitochondrial transport proteins i.e. Miro1, Miro2, TRAK1, KHC and Myo19, in MSC before and after rotenone induction. Rotenone treatment was associated with decreased expression of Miro1, while there was no effect as such on Miro2, TRAK1, KHC and Myo19 (Fig 3A). We further explored the role of Miro1 in intercellular mitochondrial donation. We first investigated the comparative expression pattern of Miro1 in MSC, lung epithelial cells (LA-4) and fibroblasts (3T3) by Western blot analysis and normalized with GAPDH (Glyceraldehyde 3-phosphate dehydrogenase) (Fig 3B). Donor mesenchymal stem cells and fibroblast cells had higher levels of Miro1 compared to recipient epithelial cells, suggesting a critical Miro1 driven kinetic model for intercellular mitochondrial transfer.

To determine whether mitochondrial transfer was indeed regulated by Miro1, we used MSC in which Miro1 had been knocked down ($MSCmiro^{Lo}$) or overexpressed ($MSCmiro^{Hi}$) (Fig 3C). The *in vitro* study involved a co-culture study of MSC with epithelial cells LA-4, which were stressed with rotenone. $MSCmiro^{Lo}$ cells were phenotypically healthy in culture, proliferated normally, had normal ATP levels and there was no change in their mtROS levels compared to control MSC. However, they were unable to transfer mitochondria to epithelial cells or to attenuate rotenone-induced epithelial mtROS production (Fig 3D and 3E) whereas scrambled shRNA-treated MSC ($MSCmiro^{Sc}$) remained effective. In contrast, overexpression of Miro1 in MSC ($MSCmiro^{Hi}$) was associated with more efficient mitochondrial transfer and inhibition of rotenone-induced epithelial mtROS than the cDNA control-transfected MSC ($MSCmiro^{Cc}$) (Fig 3D and E). Further, confocal imaging confirmed that recipient cells with high levels of donated mitochondria were the ones with maximal diminution of ROS (data not shown). Mitochondrial movement was retarded in $MSCmiro^{Lo}$ compared to $MSCmiro^{Sc}$, although TNT were formed normally (Supplementary Movie S4). Miro1 also appeared to be a critical regulator of mitochondrial donation in SMC. Overexpression of Miro1, but not another regulatory protein TRAK1, increased mitochondrial transfer in SMC (Fig 3F–H). Human SMC overexpressing Miro1 were also efficient donors (Fig 3H), suggesting that the levels of Miro1 in mesenchymal cells can be bioengineered to optimize mitochondrial donor potency. Hence, Miro1 level appeared to be a crucial component of intercellular mitochondrial transfer.

Miro1-overexpressing MSC are efficient mitochondrial donors with enhanced rescue potential

To confirm the critical role of Miro1 in mitochondrial transfer from MSC and stem cell repair potential, we conducted an *in vivo* study where we compared the effects of control MSC ($MSCmiro^{Cc}$ or $MSCmiro^{Sc}$), $MSCmiro^{Lo}$, and $MSCmiro^{Hi}$ in the mouse model of rotenone-induced mitochondrial dysfunction and airway injury. When compared to control MSC, $MSCmiro^{Lo}$ were ineffective in reducing inflammation and bronchial epithelial cell apoptosis, while $MSCmiro^{Hi}$ were more efficient (Fig 4A and B). The reduced

therapeutic efficacy of MSCmiro^{Lo} was associated with reduced mitochondrial donor capacity since MSCmiro^{Lo} were unable to transfer mitochondria to CCSP^{+} bronchial epithelial cells (Fig 4C; Supplementary Fig S5A). Functional studies in lung cytosolic extracts of MSC-miro^{Lo}-treated mice revealed increase in cytochrome c release and decreased ATP levels in total lung protein (Fig 4D and E), when compared to control MSC or MSCmiro^{Hi}, clearly indicating the critical role for mitochondrial donation.

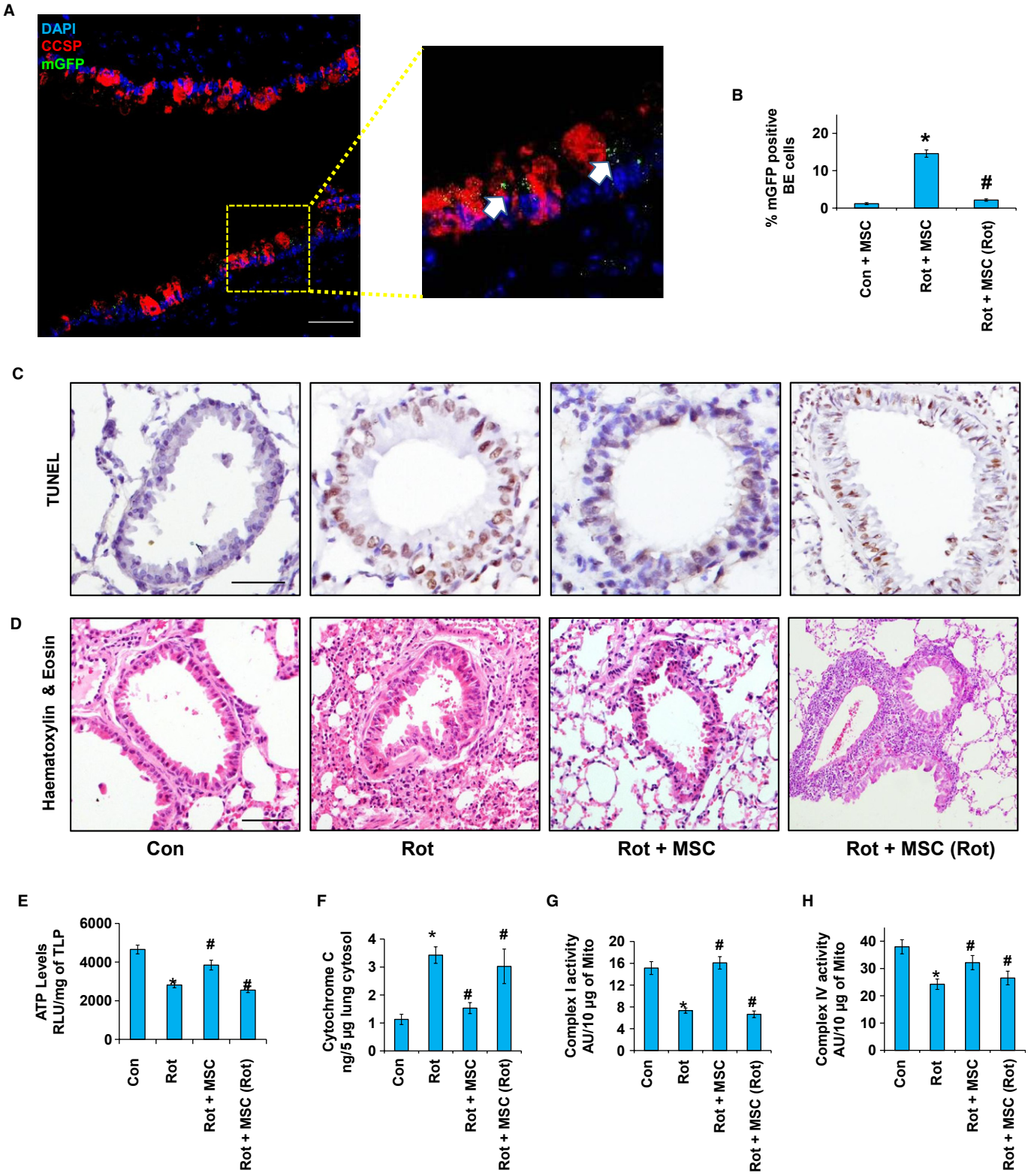

Thus, the rescue efficiency of the MSC was observed to be substantially enhanced by Miro1-overexpression, while Miro1 knockdown inhibited MSC mediated rescue of epithelial stress.

Miro1-mediated mitochondrial donation from MSC reverses airway pathology in models of allergic airway inflammation (AAI)

Mitochondrial dysfunction in epithelial cells is a known feature of asthma (Mabalirajan *et al*, 2008; Ahmad *et al*, 2012) and it triggers enhanced allergic airway inflammation (AAI) and airway remodeling in mice (Ahmad *et al*, 2011). We hypothesized that the fibroblast and smooth muscle proliferation, seen beneath the allergically inflamed bronchial epithelial layer in asthma, may represent a compensatory alternative donor response to mitochondrial deficiency of the epithelium. A mouse model of ovalbumin (OVA)-induced allergic airway inflammation (AAI) was used (Fig 5A). With increased mitochondrial dysfunction in bronchial epithelial cells of allergically inflamed lung (Mabalirajan *et al*, 2008), there appears to be marked mitochondrial biogenesis, with increased expression of TFAM (mitochondrial transcription factor A), in underlying sub-epithelial mesenchymal elongated cells in mice model of asthma (Fig 5B) (Trian *et al*, 2007). Our hypothesis predicts that exogenous mitochondrial donors should inhibit proliferation of local mesenchymal mitochondrial donor cells. In order to determine whether MSC can donate mitochondria to different lung cell populations, during asthma, double labeling was done and quantified by FACS (Fig 5C). Quantitation of mitochondrial uptake in different lung cell populations revealed a high mitochondrial uptake by EpCAM positive lung epithelial cells (EC), specifically CCSP positive BE, followed by SPC positive AE, F4/80 positive Ma and α-SMA ME. Endothelial cells and infiltrating inflammatory cells also have a minimal uptake of mGFP (data not shown). As expected, MSCmiro^{Hi} were efficient mitochondrial donors compared to control MSC, while MSCmiro^{Lo} were ineffective donors (Fig 5D). MSCmiro^{Hi} were more effective than control MSC or MSCmiro^{Lo} in attenuating airway hyperresponsiveness (Fig 5E), decreasing pro-inflammatory Th2 cytokines IL-5 and IL-13 (Fig 5F and G), and restoring ATP levels (Fig 5H). MSCmiro^{Hi} myofibroadministration in Ova mice were also associated with attenuation of structural changes in the lungs in form of decreased blast cell number (Fig 6A), inflammatory cell infiltration (Fig 6B), collagen deposition (Fig 6C) and mucus hypersecretion (Fig 6D). To validate this observation in more clinically relevant allergy models, we used mice exposed to either cockroach extract (CE) or house-dust mite (HDM) allergens (Srivastava *et al*, 2010). In each case, MSCmiro^{Hi} were more effective in attenuating AHR (Fig 7A and B) and airway remodeling than control MSC, which were more effective than MSCmiro^{Lo}. Maximal restoration of normal airway morphology was seen in MSCmiro^{Hi}-treated mice and persistence of aberrant airway morphology was seen in MSCmiro^{Lo} treated mice (Fig 7C and D). This can be vividly seen by immunohistochemical staining for airway smooth muscle/myofibroblasts (Fig 7E), Complex IV activity in mitochondrial extracts of lung (Fig 7F), levels of epithelial stress cytokine IL-25 (Fig 7G), and cytochrome c release in cytosolic extract of mice lung (Supplementary Fig S5B).

Relevance of these findings to human asthma was tested in an indirect IL-13-induced epithelial injury model. We simulated the *in vivo* asthmatic condition, where infiltrating inflammatory cells induce epithelial injury, in an *in vitro* system where human bronchial epithelial cells are treated with the culture supernatant of human mononuclear cells that have been activated by IL-13 (see Materials and Methods). Treatment of bronchial epithelial cells with such culture supernatant leads to high levels of cell stress and mtROS, comparable to *in vivo* AAI models, and greater than *in vitro* induction of bronchial epithelial cells by IL-13 (Mabalirajan *et al*, 2013). In this system, human MSCmiro^{Hi} were again more effective in mitochondrial transfer and mtROS attenuation than control human MSC, which were more effective than human MSCmiro^{Lo} (Supplementary Fig S5C and D). This confirmed that the primary mechanisms of increased rescue potential of MSCmiro^{Hi} were shared between mouse and human cells.

Thus, increased therapeutic efficiency of the Miro1-overexpressing MSC was consistently seen across multiple models of asthma both *in vivo* and *in vitro*.

Increased anti-inflammatory effects of Miro1 overexpression in MSC are related to increased epithelial repair via mitochondrial donation

We also explored whether the anti-inflammatory potential of MSCmiro^{Hi} was due to increased mitochondrial donation or due to increased secretion of anti-inflammatory molecules. Many of the therapeutic effects of MSC have been attributed to their paracrine action and secretion of immunomodulatory molecules such as, Indoleamine-pyrrole-2,3-dioxygenase (IDO), nitric oxide (NO), TGF-β,

Figure 2. *In vivo* transfer of mitochondria from exogenous MSC is critical in reversal of airway epithelial injury.

A Representative images of mGFP signals in the bronchial epithelium in rotenone (Rot) treated mice model lung sections post MSC administration. Bronchial epithelium stained with epithelial cell specific marker, CCSP (red) and DAPI (nuclei, blue), zoomed out area shows the presence of mGFP signal in CCSP^{+} cells. Scale bar, 20 μm.

B Total percent mGFP positive cells in whole lungs as quantitated by FACS, y-axis showing the percent mGFP in CCSP positive bronchial epithelium (BE) cells. The control (Con) mice treated with MSC and rotenone-induced mice(Rot) treated with rotenone-induced MSC (MSC (Rot)) were associated with a much lower number of mGFP signals in the lung BE cells compared to rotenone-induced mice treated with un-induced MSC.

C, D Representative images of TUNEL assay for apoptosis and Haematoxylin & Eosin staining for inflammation in lungs of control (con) or Rotenone-treated (Rot) mice, which were further administered with healthy MSC (Rot + MSC) or rotenone-treated MSCs (Rot + MSC (Rot)). Scale bar, 50 μm.

E Total ATP levels were measured in total lung protein (TLP), expressed as relative light units/milligram of total lung protein (RLU/mg). Rotenone (Rot) treatment led to a significant decrease in ATP levels, which was restored by MSC administration, but not by rotenone-treated MSC (MSC (Rot)).

F–H To detect recovery of mitochondrial dysfunction, cytochrome C levels were measured in lung cytosolic proteins (F), and complex I (G) and complex IV activity (H) was measured in mitochondrial extracts. The healthy MSC show suppression of cytochrome C release into cytosol and recovery of both complex I and complex IV activity, but these features deteriorated with administration of rotenone treated MSC (MSC (Rot)).

Data information: In (B) and (D–H): data are shown as mean ± s.e.m. of three independent experiments $^{*}P < 0.05$ versus Con, $^{\#}P < 0.05$, versus Rot.

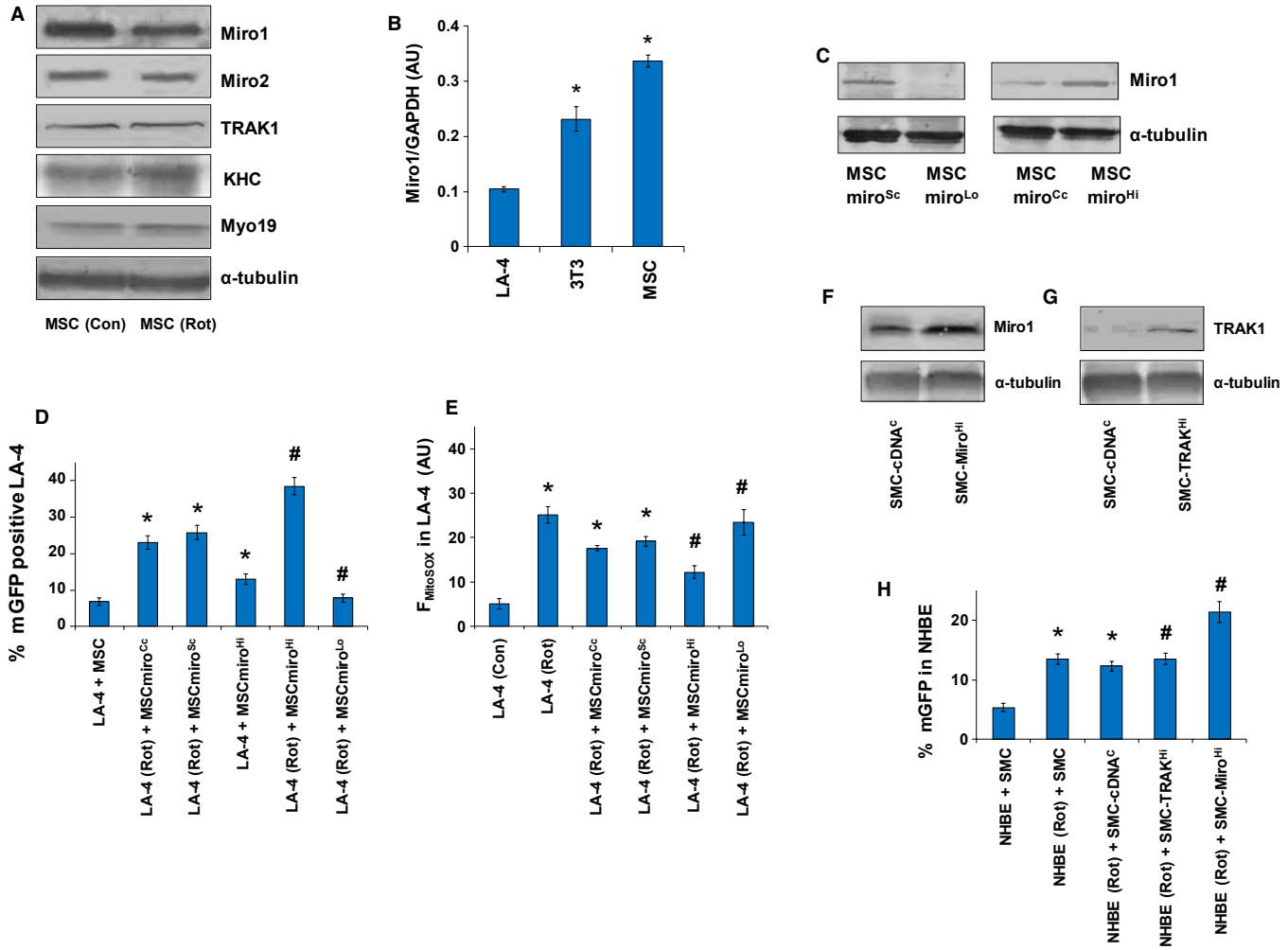

Figure 3. Miro1 overexpression enhances mitochondrial donation to injured epithelial cells.

A Western blot of Miro1, Miro2, TRAK1, KHC and Myo19 with loading control α-tubulin in MSC under control and rotenone-treated conditions; 60 μg of total cell protein was used for Western blot.

B Total cell protein prepared from different cells was used to check for the expression of Miro1. MSC expressed high levels of Miro1, as revealed by densitometry of the Western blot bands calculated by comparing the signal of Miro1 with GAPDH, in arbitrary units (AU). $^{*}P < 0.05$ versus LA-4.

C Western blot of Miro1 in MSC transfected with scrambled shRNA ($MSCmiro^{Sc}$), specific Miro1 shRNA ($MSCmiro^{Lo}$), control cDNA ($MSCmiro^{Cc}$) and specific Miro1 cDNA ($MSCmiro^{Hi}$) with 30 μg of total cell protein per lane and α-tubulin used as loading control.

D Quantitative FACS measurement of total percentage of mitochondria in LA-4 donated by mGFP-transfected naive MSC and Miro1-modulated MSC. MSC with upregulated expression of Miro1 ($MSCmiro^{Hi}$) show a high efficient transfer of mitochondria to rotenone-stressed LA-4 as compared to normal MSC ($MSCmiro^{Cc}$ and $MSCmiro^{Sc}$); whereas MSC with Miro1 knock-down ($MSCmiro^{Lo}$) fail to transfer mitochondria to rotenone-stressed LA-4 cells. $^{*}P < 0.05$ versus LA4 + MSC, $^{\#}P < 0.05$ versus LA-4(Rot) + $MSCmiro^{Cc}$ or $MSCmiro^{Sc}$.

E Quantitative FACS measurement of total mitochondrial ROS (mtROS) in LA-4 cells after co-culture with MSC. Control cDNA MSC ($MSCmiro^{Cc}$) or control shRNA MSC ($MSC\text{-}miro^{Sc}$) were associated with attenuation of mtROS levels in LA-4 cells compared to rotenone-treated LA-4 cells. In both cases, Miro1 upregulation in MSC ($MSCmiro^{Hi}$) further attenuated mtROS levels, while Miro1 knockdown MSC ($MSCmiro^{Lo}$) did not show any protective effect. $^{*}P < 0.05$ versus LA4 (Con), $^{\#}P < 0.05$ versus LA-4 (Rot) + $MSCmiro^{Cc}$ or $MSCmiro^{Sc}$.

F, G Western blot analysis for expression of Miro1 (F) and TRAK1 (G). Miro1 was measured in SMC transfected with control cDNA ($SMC\text{-}cDNA^{C}$) and specific Miro1 cDNA plasmid ($SMC\text{-}Miro^{Hi}$). TRAK1 was measured by Western blot in SMC transfected with control cDNA ($SMC\text{-}cDNA^{C}$) and TRAK1 overexpression plasmids ($SMC\text{-}TRAK1^{Hi}$). Total cell protein prepared from SMC was used and α- tubulin was used as a loading control.

H FACS measurement of transfer of mitochondria estimated by percentage counts of mGFP (from mGFP transfected SMC) in NHBE cells. Miro1 upregulation was associated with increased mitochondrial transportation from SMC ($SMC\text{-}Miro^{Hi}$) compared to rotenone (Rot)-treated or control-cDNA transfected cells ($SMC\text{-}cDNA^{C}$). TRAK1 overexpressed SMC ($SMC\text{-}TRAK1^{Hi}$) did not show any significant mitochondrial transfer compared to control cDNA-transfected cells ($SMC\text{-}cDNA^{C}$). Data is shown as mean ± s.e.m. of three independent experiments $^{*}P < 0.05$ versus NHBE + SMC, $^{\#}P < 0.05$ versus NHBE (Rot) + $SMC\text{-}cDNA^{C}$.

Source data are available online for this figure.

IL-10 and PGE2 (Ren *et al*, 2008). We therefore measured the effect of Miro1 overexpression on the secretion of such molecules by MSC during inflammatory conditions. IFN-γ and TNF-α were used to induce the secretion of anti-inflammatory molecules by MSC (Lambrecht & Hammad, 2012). We found that in presence of IFN-γ and TNF-α, MSC secrete NO, TGF-β and PGE2, but no significant differences

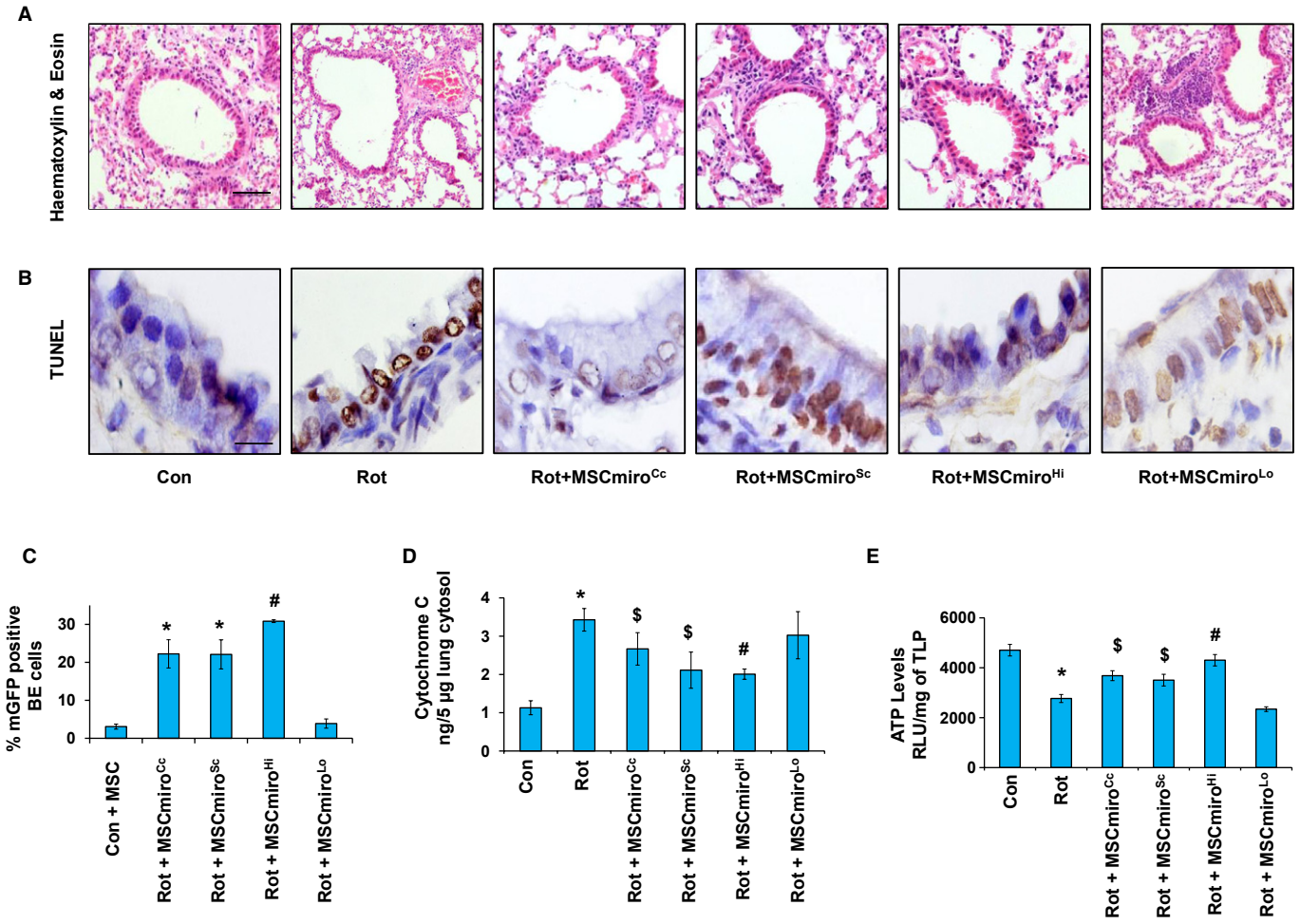

Figure 4. Restoration of mitochondrial bioenergetics by Miro1-overexpressing MSC.

A, B Representative images of inflammatory cell infiltration and epithelial cell apoptosis. Both cellular infiltration and apoptosis were significantly decreased in mice lungs treated with MSCmiro^{Hi} while there was no effect with MSCmiro^{Lo}. Scale bars, 50 µm (A) and 10 µm (B).

C Percent of total mGFP in bronchial epithelial cells after treatment with mGFP transfected MSC as indicated. Miro1-overexpressing MSC (MSCmiro^{Hi}) were more efficient mitochondrial donors compared to control cDNA-transfected MSC (MSCmiro^{Cc}). Miro1 knockdown MSC (MSCmiro^{Lo}) have a decreased mitochondrial donation potential compared to control shRNA transfected cells (MSCmiro^{Sc}).

D, E MSCmiro^{Hi} treatment significantly decreased cytochrome c release (D) and restored ATP levels (E) compared to control-transfected MSC (MSCmiro^{Cc}), while MSCmiro^{Lo} were less effective.

Data information: In (C-E), data are shown as mean ± s.e.m. of three independent experiments, *$P < 0.05$ versus Con, $^{\$}P < 0.05$ versus Rot and $^{\#}P < 0.05$, versus Rot, MSCmiro^{Cc} or MSCmiro^{Sc}.

were seen between control MSC and MSCmiro^{Hi} (Table 1). The results indicated that the increased therapeutic effects of MSCmiro^{Hi} were not due to any changes in their general secretory properties. Since epithelial cells can also orchestrate inflammation by secreting pro-inflammatory cytokines like TSLP, IL-25 and IL-33 (Swamy *et al*, 2010), we conjectured that increased mitochondrial donation by MSC-miro^{Hi} may reduce epithelial injury and thereby reduce pro-inflammatory epithelial cytokines. For this, the bronchial epithelial cells from lungs of MSCmiro^{Cc} and MSCmiro^{Hi}-treated Sham and Ova mice groups were selectively isolated using laser capture microdissection (LMD; Zeiss) and relevant cytokines, i.e. TSLP, IL-25 and IL-33, were measured in the cell lysates (Lambrecht & Hammad, 2012). We found that MSCmiro^{Hi} treatment was associated with a significant decrease in the expression of TSLP, IL-25 and IL-33 (Fig 8A–C), and restoration of normal mitochondrial morphology as observed in mice lung tissue sections on transmission electron microscope (Fig 8D). Moreover, Ova-treated lung epithelium showed fragmented dysfunctional mitochondria which were partially recovered with MSCmiro^{Hi} treatment. Notably, both nanotubes and MSC were required for the therapeutic effect of Miro1 overexpression. Knockdown of TNFAIP2 in MSCmiro^{Hi} greatly reduced both mitochondrial transfer and mtROS inhibition *in vitro* and significantly attenuated the therapeutic effect in a mouse asthma model (Supplementary Fig S6). Overexpression of Miro1 *in vitro* in epithelial cells or in mouse lungs was not associated with any change in either mtROS or AAI (Supplementary Fig S7).

Overall, these results confirmed that MSCmiro^{Hi} treatment is associated with greater mitochondrial donation via nanotubes,

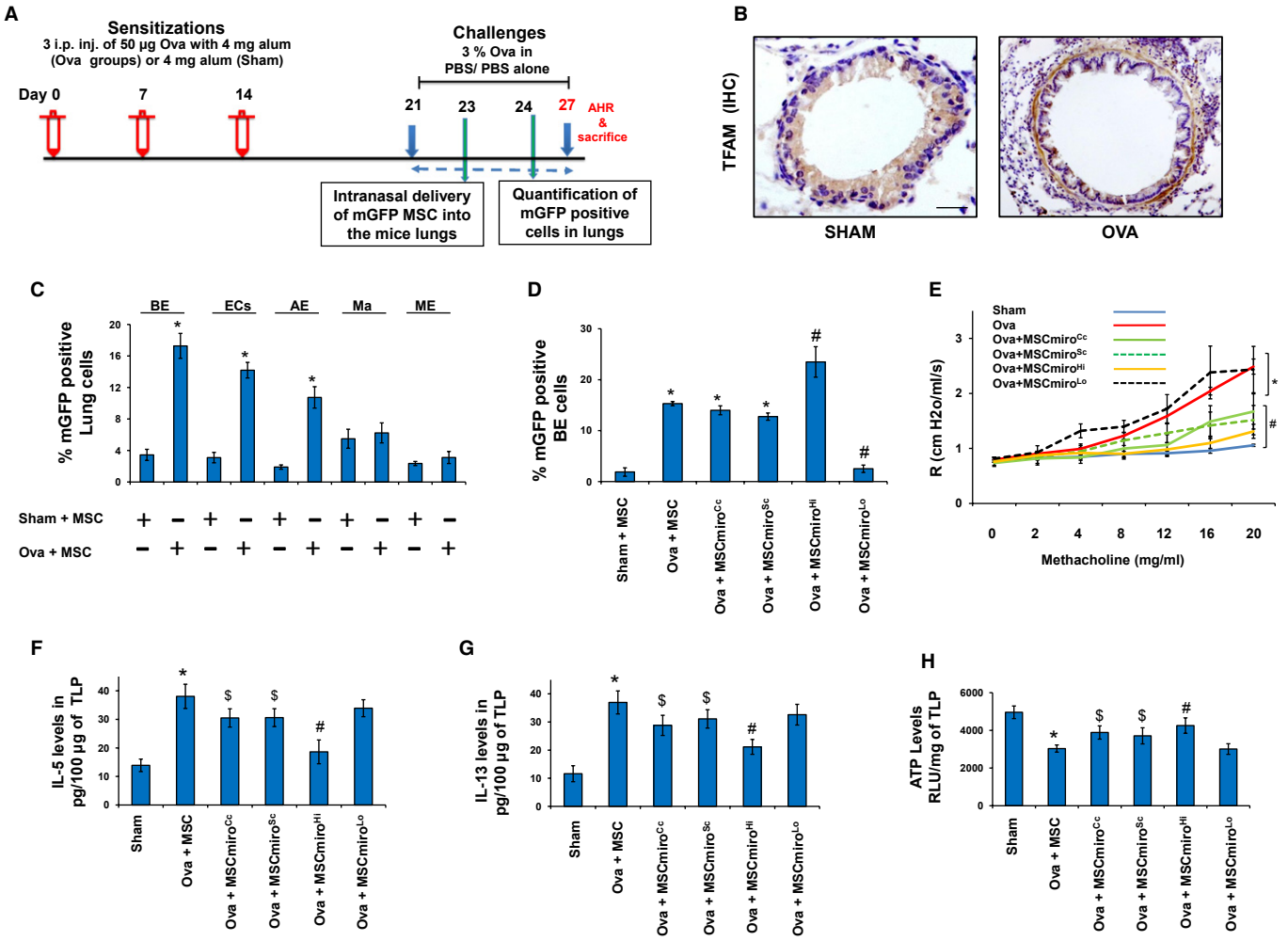

Figure 5. Miro1-overexpressing MSC are better mitochondrial donors to asthmatic airways.

A Scheme for development of acute mouse model of asthma and delivery of mGFP labeled MSC into the mice lungs. Mice were Ova-sensitized with weekly 3 successive intraperitoneal (i.p.) injections of ovalbumin (50 µg) allergen and then intranasally challenged with 3% aerosolized ovalbumin for a week on alternate days to develop acute airway allergy. MSC were injected after two challenges on 23rd day post ovalbumin challenge and further after subsequent challenges, the mice were sacrificed.

B Representative images of TFAM expression in mice lungs. Increased mitochondrial biogenesis indicated by higher expression of TFAM in Ova mice compared to Sham as indicated by immunohistochemistry for TFAM. Scale bars, 50 µm.

C Percentage of mGFP in different cell populations of the mice lung under normal and Ova condition treated with MSC, quantified by FACS. BE, bronchial epithelial cells stained with CCSP; ECs, epithelial cells stained with EpCAM; AE, alveolar epithelial cells stained with SPC; Ma, macrophages stained with F4/80; ME, mesenchymal cells stained with alpha smooth muscle actin.

D Percentage of mGFP signal in bronchial epithelial cells as quantified by FACS. Treatment with Miro1-overexpressing MSC ($MSCmiro^{Hi}$) significantly increased percentage of mGFP positive cells, while Miro1 knockdown MSC ($MSCmiro^{Lo}$) was associated with decreased mGFP positive cells compared to control-cDNA or control shRNA-treated cells.

E Airway hyperresponsiveness (AHR) was significantly increased in Ova and shows no improvement with administration of $MSCmiro^{Lo}$. $MSCmiro^{Hi}$ treatment led to a significant decrease in AHR compared to Ova mice or Ova mice treated with control MSC ($MSCmiro^{Cc}$, $MSCmiro^{Sc}$).

F, G IL-5 and IL-13 were significantly upregulated in Ova mice compared to Sham mice. $MSCmiro^{Hi}$ treatment significantly decreased the levels of both inflammatory cytokines, while there was no effect with administration of $MSCmiro^{Lo}$.

H ATP levels were significantly decreased in Ova mice compared to Sham mice. Miro1 overexpressing MSC ($MSCmiro^{Hi}$) significantly restored ATP levels, while there was no effect with Miro1-downregulated MSC ($MSCmiro^{Lo}$).

Data information: In (C-H): data are of two independent experiments, $^{*}P < 0.05$ versus Sham, $^{\$}P < 0.05$ versus Ova and $^{\#}P < 0.05$ versus Ova, Ova + $MSCmiro^{Cc}$ or Ova + $MSCmiro^{Sc}$.

greater rescue of injured epithelial cells, critical reduction in epithelial mediated amplification of the immune response, and ultimately superior therapeutic efficacy in models of asthma. The proposed model of Miro1 mediated mitochondrial donation by MSC to rescue epithelial function is thus summarised in a schematic diagram (Fig 8E). It also indicates feasibility of a novel approach of using mitochondrial engineered mesenchymal stem cells for better therapeutic results in asthma and other lung diseases with epithelial injury.

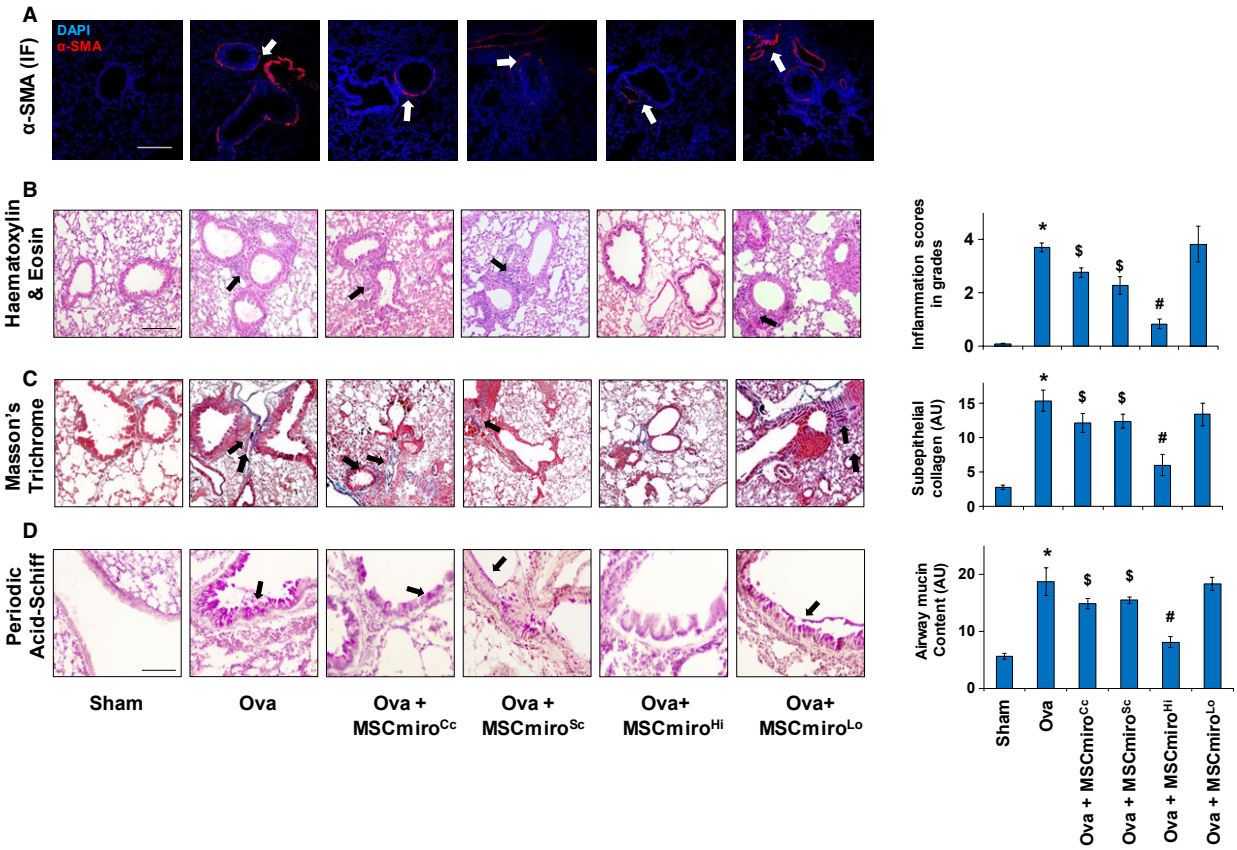

Figure 6. Miro1-overexpressing MSC, a better therapeutic for asthma.

A Representative images of alpha smooth muscle actin (α-SMA) staining (red) indicate myofibroblast cells (white arrows) in lungs of control mice (Sham), ovalbumin-treated mice (Ova), mice with ovalbumin control MSC-treated cells (MSCmiro^{Cc} or MSCmiro^{Sc}), Miro1-overexpressed MSC (MSCmiro^{Hi}) and Miro1-downregulated MSC (MSCmiro^{Lo}). MSCmiro^{Hi} treatment led to a significant decrease in the number of myofibroblast cells, while there was no effect with MSCmiro^{Lo} treatment.

B Representative images of Haematoxylin & Eosin stained lung sections. MSCmiro^{Hi} significantly decreased the cellular infiltration (indicated by black arrows) in the ovalbumin treated mice lungs compared to the only Ova mice, while there was no effect observed with MSCmiro^{Lo}. Inflammation scoring was done to quantify the degree of cellular infiltration (perivascular and peribronchial), as shown in the bar graph (right side).

C Masson's trichrome stain was used for staining collagen (blue) in mice lungs. Ova mice had increased collagen deposition (indicated by black arrows) beneath the bronchial epithelium and vessel wall compared to Sham mice. MSCmiro^{Hi} treatment led to a significant decrease in collagen deposition, MSCmiro^{Lo} did not show any decrease compared to Ova mice. Total collagen content measured by image quantitation revealed significant decrease in collagen content by MSCmiro^{Hi} treatment, while as control cDNA or shRNA-transfected MSC (MSCmiro^{Cc} or MSCmiro^{Sc}) also showed a modest improvement, as shown in the bar graph (right side).

D Mucin content (pink-purple) in mouse lungs was measured by Periodic acid-Schiff stain. MSCmiro^{Hi} treatment led to a significant decrease in mucus secretion, as seen with observed mucin granules (indicated by black arrows) while as MSCmiro^{Lo} treatment did not, compared to Ova mice. Control cDNA or shRNA-transfected MSC (MSCmiro^{Cc} or MSCmiro^{Sc}) also showed a modest improvement. Total mucin content was measured by image quantitation, as shown in the bar graph (right side).

Data information: Data in (B–D) are representative of two independent experiments, $^{*}P < 0.05$ versus Sham, $^{\$}P < 0.05$ versus Ova and $^{\#}P < 0.05$ versus Ova, Ova + MSCmiro^{Cc} or Ova + MSCmiro^{Sc}; scale bars, 10 μM (A), 50 μM (B, C) and 30 μM (D).

Discussion

Mitochondrial transfer from stem cells is associated with rescue of aerobic respiration and restoration of mitochondria function in the recipient cells (Spees *et al*, 2006; Islam *et al*, 2012). Here we show for the first time that mitochondrial transfer is directly responsible for the *in vivo* benefits of mesenchymal stem cell therapy in models of airway injury and inflammation. We also partially elucidate the molecular mechanisms by which mitochondrial transfer happens and show that these stem cells can be engineered to create more effective therapies.

Prior to our work, the mechanisms of mitochondrial donation by stem cells were unclear, with tunneling nanotubes (TNT) shown *in vitro* (Vallabhaneni *et al*, 2012) and formation of both nanotubes and mitochondria containing microvesicles *in vivo* (Wang *et al*, 2010; Islam *et al*, 2012). Whether mitochondrial transport was part of a general exchange of cellular contents or a specific directed movement, was also unclear. Our data show that the movement of mitochondria from stem cells to recipient cells is regulated by Miro1 and is part of a well-directed process, rather than a general exchange of contents. It is anticipated that Miro1-mediated movement of mitochondria will be via microtubules across cytoplasmic bridges such as TNT. Apart from direct *in vitro* imaging of mitochondrial transfer via TNT, we found that lentiviral-mediated knockdown of TNFAIP2, a protein responsible for the formation of TNT (Hase *et al*, 2009), led to abolishment of mitochondrial transfer and substantial reduction of therapeutic effect (Supplementary Fig S1C and S5). We have further seen that lack of Miro1 does not prevent formation of TNT, but mitochondrial

Figure 7. Therapeutic effects of Miro1-overexpressing MSC in Cockroach-extract and HDM-extract induced models of AAI.

A, B Airway hyperresponsiveness (AHR) was significantly increased in CE and HDM mice models, which was not improved with MSCmiro^{Lo} treatment. MSCmiro^{Hi} treatment led to a significant decrease in AHR compared to CE or HDM mice as well as CE or HDM mice treated with control MSC (MSC (con)).

C, D Representative images of Haematoxylin & Eosin staining for detection of inflammation (red arrows) in lungs of the CE mouse model treated with MSC show reduction of inflammation with MSCmiro^{Hi} that is much more efficient compared to MSC-con treatment, whereas there is persistent inflammation with MSCmiro^{Lo} treatment.

E Representative images of alpha smooth muscle actin (α-SMA) immunohistochemistry staining indicates myofibroblast cells in mice lung sections. There is an increase in expression of α-SMA (brown stained regions indicated with red arrows) in CE-induced mice (CE), as well as CE mice treated with MSCmiro^{Lo}, but a sufficient reduction with control MSC (MSC (con)), and a high reduction when treatedwith MSCmiro^{Hi}.

F Complex IV activity measured in mitochondrial extract of lung samples from the CE allergen mouse model, showing significant recovery of COX IV activity when CE mice were treated with MSCmiro^{Hi} as compared to moderate rescue by MSC (con) and almost no rescue with MSCmiro^{Lo} treatment.

G Levels of epithelial stress cytokine IL-25 as measured in lung samples from the CE allergen mouse model, show efficient reduction when CE mice were treated with MSCmiro^{Hi} as compared to moderate decrease with MSC (con) and almost no reduction with MSCmiro^{Lo} treatment.

Data information: In (C–E): scale bar, 50 μm. In (A–B, F–G): $^{*}P < 0.05$ versus Sham; $^{\#}P < 0.05$ versus CE or HDM.

movement through these tubes is majorly retarded (Supplementary Movie S4). However, we could see uncharacterized vesicular structures moving through the tubes, which is consistent with the current view of Miro1 as a specific regulator of mitochondrial motility. The loss of MSC mitochondrial motility was associated with loss of MSC-mediated rescue of epithelial cell injury, both *in vitro* and *in vivo*. Labeled mitochondria from MSC were definitively visualized within airway epithelial cells and also tracked to other lung cell populations. While we did not visualize the actual moment of transfer of mitochondria *in vivo* (Islam *et al*, 2012), our data is the most definitive evidence to date that mitochondrial donation is a critical and regulated aspect of MSC function. In our studies, Miro1 was essential for stem cell associated benefit, suggesting that mitochondrial transport via microtubules (across cytoplasmic bridges) is an important stem-cell function. Any important role for stem cell differentiation appears unlikely in our model, because of the early time points and dependency on the mitochondrial transport system. Also, the double positive cells during microscopy were strongly CCSP positive Clara cells, which were also weakly positive for mGFP labeled mitochondria from MSC. The expected phenotype of a differentiating stem cell, i.e. strongly mGFP positive cell with some CCSP positivity, was not seen. Similarly, secretion of important anti-inflammatory molecules by MSC was unrelated to Miro1 expression, excluding the possibility that altered efficacy of MSC function relates to increased secretory function. Also, in our model we did not see significant effects of cultured MSC supernatant (Supplementary Fig S1G), excluding a major role for secreted products. However, a more detailed analysis of the secretome could uncover useful differences.

Taken together, this is the first evidence of a regulated mitochondrial transport system in stem cells that directs intercellular mitochondrial trafficking. We also provide the first evidence that this machinery exists in other cells of mesenchymal origin such as smooth muscle cells and fibroblasts. It should be noted that these cells are low efficiency donors with negligible repair effects (Fig 1D and G). However, this may be enhanced by Miro1 overexpression (Fig 3F). We speculate that proliferation of fibroblasts/myofibroblast cells in lung injury, leading to remodeling, is part of a concerted compensatory repair response including mitochondrial donation. While we have no direct evidence supporting this, we did note that, (i) mitochondrial biogenesis is strongly activated in such cells during asthmatic airway remodeling (Fig 5B); (ii) exogenous administration of stem cells leads to donation of mitochondria and inhibition of airway remodeling (Fig 6A–D); (iii) MSCmiro^{Lo} stem cells lacking mitochondrial donor capacity, but fully normal in other respects, show minimal efficacy in attenuating either airway hyperresponsiveness or remodeling; (iv) MSCmiro^{Hi} cells, with increased mitochondrial transfer efficiency, inhibit airway hyperresponsiveness and remodeling (Fig 5E and 6A–D). Since the differential labeling of mitochondria of different cell lineages *in vivo* is not plausible yet, we were unable to study this further. Lineage specific *in vivo* studies are needed for further understanding. It is also important to define the regulatory system on the recipient side, which presumably initiates the mitochondrial transfer, since there is minimal transfer to unstressed epithelial cells, and may determine the extent. Variability in the number of MSC mitochondria received by different epithelial cells was quite high in our study, ranging from barely visible to being greater than the native mitochondria (see Fig 1E and F, Supplementary Images file in accompanying Dataset 3). While it would be efficient for these systems to be related to stress signaling rather than stochastic, further research is needed.

In summary, Miro1 regulated mitochondrial movement from stem cells to stressed recipient epithelial cells is a critical aspect of stem cell therapeutics. Molecular engineering of stem cell mitochondrial transport machinery by overexpressing Miro1 increases their mitochondrial donor capacity and thereby beneficial effects in lung injury and asthma. Further understanding of this pathway may translate into better stem cell therapy.

Materials and Methods

Cell lines

Cell lines (Human bronchial epithelial cells, BEAS-2B; alveolar epithelial cells, A549; mouse lung epithelial cells, ML-12; mouse lung adencarcinoma cells LA-4; Human Peripheral Blood Monocytes, THP-1) and mouse fibroblasts (NIH/3T3) were purchased from either ECACC or ATCC, and maintained as recommended. Primary normal human bronchial epithelial cells (NHBE) and bronchial smooth muscle cells (SMC) were purchased from Lonza (Switzerland).

Isolation of mesenchymal stem cells and primary mouse tracheal epithelial cells

Human bone marrow-derived mesenchymal stem cells (hMSC) were gifted from National Center for Cell Science, Pune. Mouse mesenchymalstem cells (MSC) were isolated from Balb/c mice by minor

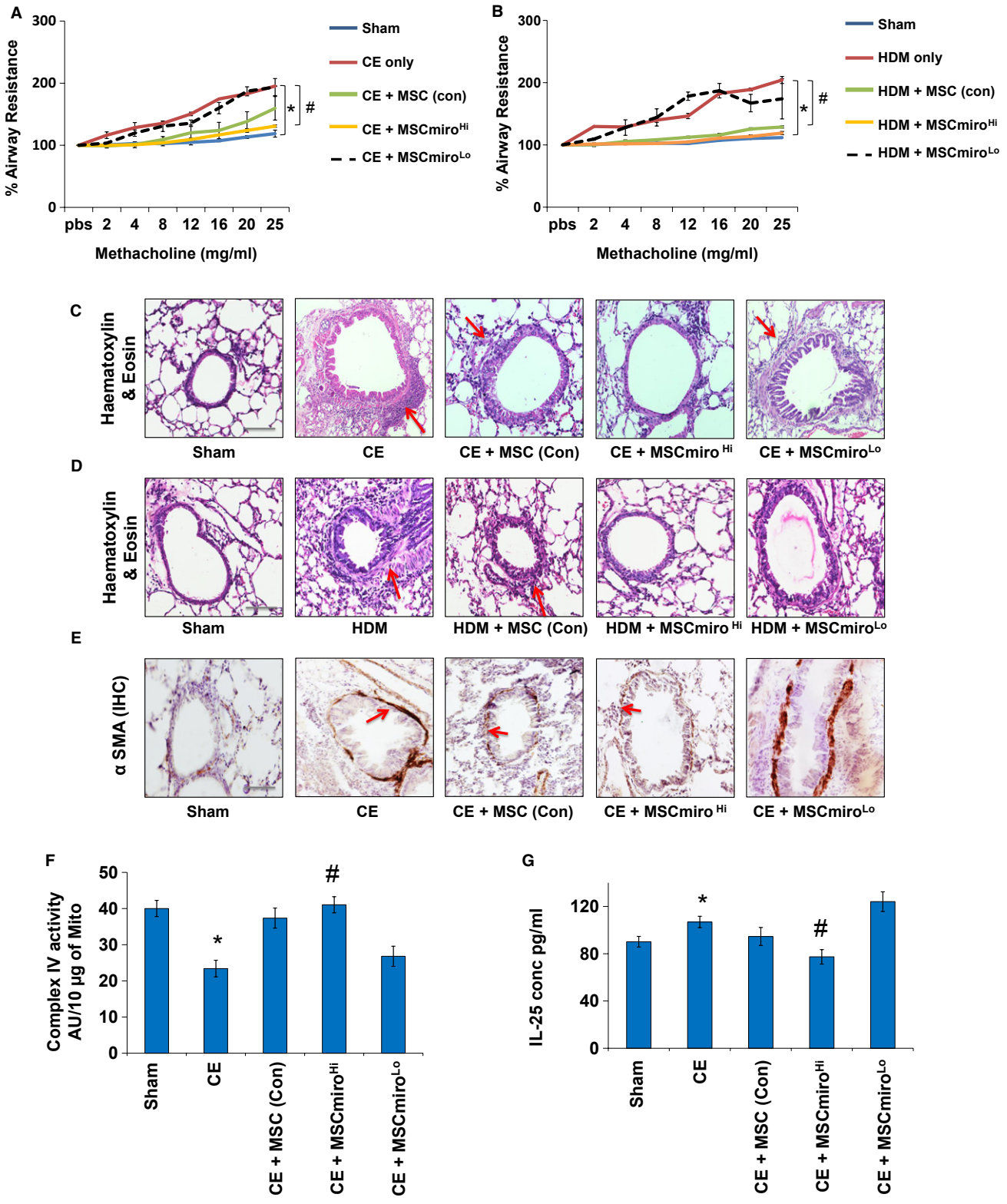

modifications of the protocol (Zhu *et al*, 2010) with marrow-derived cells cultured in Mesencult (Stem Cell Technologies, Canada), a defined selective growth medium for mouse mesenchymal stem cells. The primary cells were cultured in a plating density of 10^6 cells/ml in T25 culture flasks, and all experiments were performed in third/fourth passages. The mesenchymal stem cells were characterized by the expression of specific markers like CD105, CD44 and Sca-1 (Supplementary Fig S2C).

Table 1. Quantification of immunomodulatory molecules secreted by MSCs with or without Miro1 overexpression after induction with IFN-γ and TNF-α

	Con	MSCmiro^{Cc}	MSCmiro^{Hi}	IFN-γ +TNF-α	IFN-γ + TNF-α +MSCmiro^{Cc}	IFN-γ + TNF-α +MSCmiro^{Hi}
TGF-β (pg/ml)	140.13 ± 10.23	135.12 ± 8.12	136.54 ± 4.67	187.5 ± 9.98*	176.8 ± 6.04	188.9 ± 6.12
IDO (pg/ml)	1.203 ± 0.589	1.259 ± 0.989	1.178 ± 0.554	1.988 ± 0.798	1.895 ± 0.823	1.909 ± 0.1234
PGE2 (pg/ml)	80.2 ± 7.43	90.32 ± 6.31	85.43 ± 7.09	221.34 ± 8.56*	212.9 8 ± 7.78	205.12 ± 12.11
NO (AU)	12.4 ± 0.98	13.5 ± 1.21	11.9 ± 1.67	45.7 ± 3.67*	43.2 ± 3.98	42.9 ± 4.12

Data are represented as Mean ± s.e.m.
*Denotes $P < 0.05$ versus Con.

Primary mouse tracheal epithelial cells (mTEC) were isolated from Balb/c mice and cultured in growth factor-supplemented complete BEBM media (Lonza) (Aich *et al*, 2012).

Fluorescent probes and dyes

Phalloidin was used to label TNT containing F-actin, between cells; similarly DiL was used for visualizing TNT between the cells. Mitotracker red/green dyes, MitoSOX red and mitochondrial specific GFP/RFP fusion proteins (Life Technologies, USA) were used for labeling mitochondria. Actin RFP, tubulin GFP, plasma membrane GFP were all purchased from Invitrogen (USA) and used as per the manufacturer's protocol.

Stress inducers

Rotenone and antimycin were purchased from Sigma (USA) and used at 100 nM concentrations. For co-culture experiments, rotenone-treated epithelial cells (6 or 12 h of induction with rotenone), were co-cultured with MSC or SMC. TNF-α (R&D Systems, USA) was used at a concentration of 20 ng/ml. THP-1 monocytes differentiated by PMA induction were induced with 25 ng/ml IL-13 (R&D Systems, USA) for 24 h and the cell conditioned media was added into BEAS-2B to trigger inflammatory response and then after 24 h assayed or co-cultured with MSC.

Transfection plasmids and constructs

Miro1, TRAK1 overexpression plasmids, Miro1 shRNA and untargeted scrambled shRNA and control cDNA plasmids were purchased from Origene (USA) and Sigma Aldrich (USA). Transfection experiments were done with Lipofectamine LTX Plus (Invitrogen) as per the manufacturer's protocol. Lentiviral plasmids for TNFAIP2 and control shRNA were purchased from Sigma (Sigma Aldrich, USA) and used as per the recommended conditions with a standardised MOI (multiplicity of infection) of 5.

Mice models

Balb/c mice (8–10 weeks old, National Institute of Nutrition, Hyderabad, India) were obtained and all procedures were reviewed and approved by the Institutional Animal Care and Ethics Committee. A novel rotenone induced mice model of epithelial cell injury and intratracheal delivery of MSC was developed, as shown in the schematic diagram (Supplementary Fig S3A). To identify the best dose at which the drug is effective in inducing mitochondrial dysfunction specifically in bronchial epithelial cells, but does not have lethal effects, different concentrations of rotenone 0.3, 3 mg and 30 mg/kg body weight (BW), were used at different time points (Supplementary Fig S3A). Finally a dose of 0.3 mg/kg BW of rotenone was selected and used for further experiments (Supplementary Fig S3A). Rotenone was prepared by dissolving in either ethanol or DMSO, and delivered by either intratracheal or intranasal route, while ethanol or DMSO was used as vehicle control. Mitochondrial GFP-transfected MSC were delivered into the mice by intratracheal or intranasal route (1×10^6), 12 h post rotenone administration. MSC were also delivered by intravenous route, 12 h post rotenone administration, but most of the data shown are with MSC delivered by intratracheal route, if not stated. For intratracheal delivery mouse were anesthetized by using a combination of either xylazine (10 mg/kg BW) or ketamine (50 mg/kg BW) or isoflurane. Mouse trachea was first visualized by video arthoscopy (Karl Storz endoskope) and then 50 μl of Rotenone or MSC were injected via an 18 gauge needle (Supplementary Movie S3). For control experiments 50 μl of diluted ethanol or media was used. For intranasal delivery mice were anesthetized by isoflurane and then MSC were delivered in 30 μl of media.

Acute mice models of asthma were developed as described earlier (Srivastava *et al*, 2010; Ahmad *et al*, 2011). For tracking mitochondrial transfer in asthma model, mice were sensitized as described earlier (Ahmad *et al*, 2011) and challenged for seven consecutive days, while MSC were delivered on 3rd day by intranasal route and mice were dissected on 5th day for visualization of mitochondrial uptake by bronchial epithelial cells or on 8th day for measurement of biochemical, physiological and histopathological parameters. Mice were grouped as Sham mice with PBS sensitization and challenge, Ova mice with ovalbumin (Sigma, USA), sensitization and challenge. Sensitization was done with three intraperitoneal (i.p.) injections of ovalbumin in the presence of alum as an adjuvant for Ova mice, while only alum in PBS was used for Sham mice. Mice administered with MSC were grouped as per the transfections done in MSC. MSC were administered 2 h before every allergen challenge. The cockroach extract allergen-induced model was developed according to established protocol (Srivastava *et al*, 2010). The house dust mite allergen (Credisol)-induced experimental asthma mouse model was developed with intra-peritoneal sensitizations and subsequent intra-nasal challenges of HDM (1.25 μg/kg body weight of mouse).

Quantitation of mtROS by FACS

Mitochondria-specific reactive oxygen species (mtROS) measurement was done by using a ROS measuring dye, MitoSOX red (Life

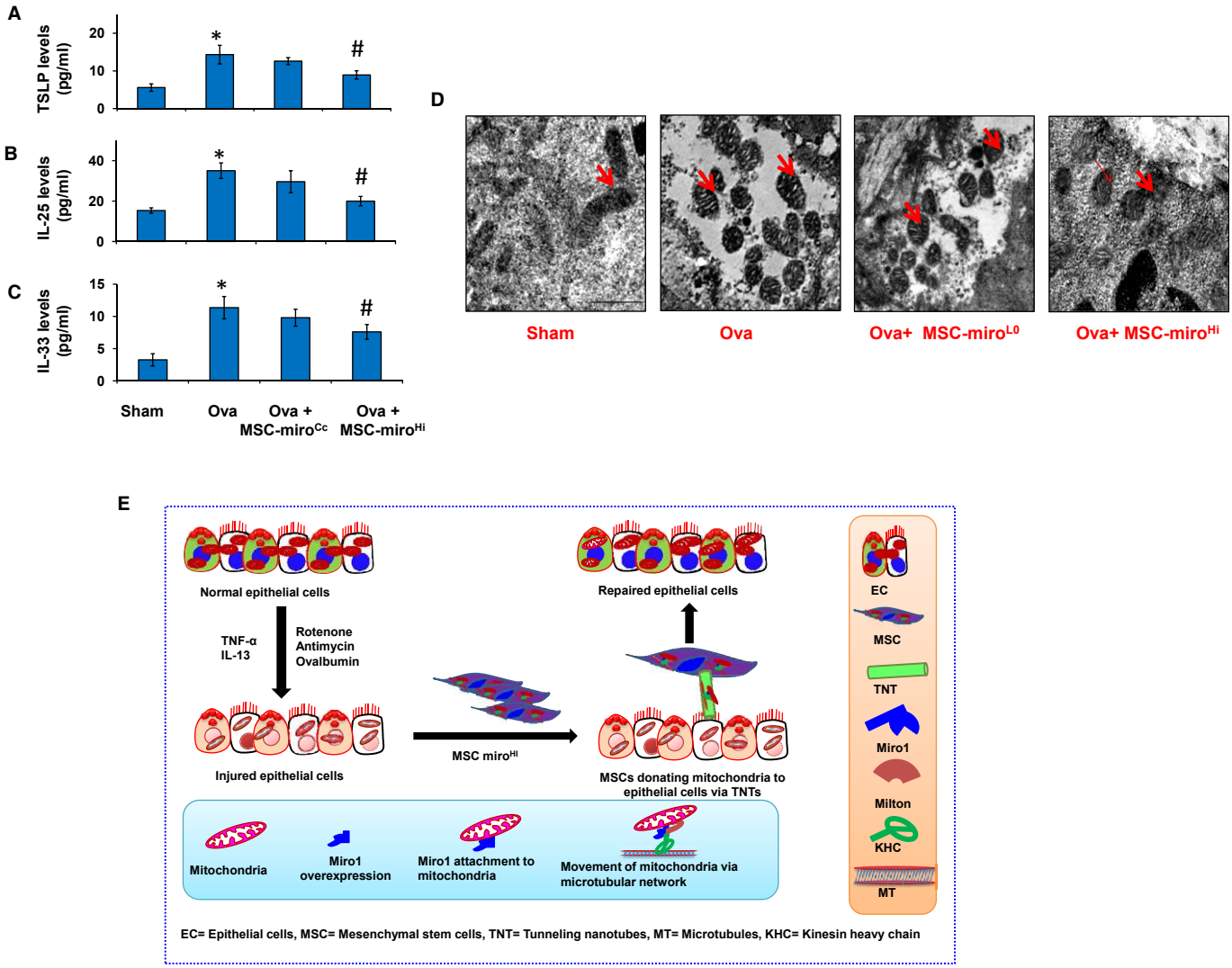

Figure 8. Miro1-overexpressing MSCs repair bronchial epithelial cell injury.

A–C ELISA data for TSLP (A), IL-25 (B) and IL-33 (C) measured in total protein, prepared from LMD-dissected bronchial epithelial cells from mice groups of Sham, Ova, Ova + MSCmiro^{Cc} and Ova + MSCmiro^{Hi}. Data are represented as mean ± s.e.m. of three independent experiments; *$P < 0.05$ versus Sham, and $^{\#}P < 0.05$ versus Ova, Ova + MSCmiro^{Cc}.

D Representative electron microscopy (EM) images of Sham, Ova, Ova with MSC-downregulated Miro1 (Ova + MSCmiro^{Lo}) and Ova with MSC-overexpressed Miro1 (Ova + MSCmiro^{Hi}) administered to mice lungs. The red arrows indicate the morphological state of mitochondria, deformations in intact mitochondrial morphology in Ova is not improved with MSCmiro^{Lo} treatment but improved with MSCmiro^{Hi} treatment. Scale bar, 0.5 μm.

E A schematic diagram showing tunneling nanotubes (TNT) formation between injured epithelial cells and MSC and the donation of mitochondria by the later to the former via these TNT.

technologies, USA). For measuring the mtROS in epithelial cells (BEAS-2B, NHBE, LA-4 and mTEC) with or without treatment, cells were stained under live conditions, co-cultured with or without MSC or mesenchymal cells, and after 24 h cells were stained with MitoSOX Red and mitochondrial ROS measurement was done in gated epithelial cells, total ROS intensity of epithelial cells was measured by gating on only epithelial cells at 0 and 24 h post co-culture. The data were presented as the total mean fluorescent intensity of MitoSOX ($F_{MitoSOX}$) in case of imaging and as the percentage-gated fluorescence shift in the histogram plot for MitoSOX ($F_{MitoSOX}$), detected with FL2 detector using BD FACS Caliber.

Flow cytometry and isolation of mouse lung cells

Quantification of mitochondrial transfer from MSC to different cell types was done by flow cytometry. In *in vitro*, MSC were labeled with mGFP and LA-4 cells with an epithelial cell specific marker, EpCAM (epithelial cell adhesion marker), also called CD326 conjugated to Alexa Fluor 633. Quantification was done by gating the EpCAM positive epithelial cells in FACS dot plot on FL4 window and mGFP signal for the gated cell population was measured on FL1 using the histogram peaks. EPs were first induced with rotenone for 12 h and then co-cultured with MSC. Mitochondrial transfer was measured after 24 h of coculture.

For *in vivo* study, mitochondrial GFP transfected MSC (mGFP) were delivered into the mice lungs by either intratracheal or intranasal route. In order to determine the mitochondrial transfer from MSC to different lung cell populations, FACS measurement was done. Lung tissues were homogenized with tissue dissociator (Miltenyi) and single-cell suspensions were prepared using lung single cell dissociation kit (Miltenyi Biotec) or in PBS. Different lung cell markers were used to quantify the mitochondrial transfer. Bronchial epithelial cells were labeled with EpCAM (Abcam) or CCSP (Abcam), alveolar cells with SPC (Santa Cruz Biotechnology), endothelial cells with VE cadherin (Santa Cruz Biotechnology), mesenchymal cells with α-SMA or fibroblast-specific protein (Abcam), macrophages with F4/80 (Abcam) and granulocytes with GR-1 (R&D). Lungs cells prepared and stained and analysed by FACS. Different lung cell populations were gated on the basis of their marker proteins on FL4 window in FACS dot plot and quantification was done on the FL1 window.

Immunocytochemistry and immunofluorescence

Cells were transfected with either mGFP (mitochondrial GFP) or mRFP (mitochondrial RFP) for 24 h before fixation with 2% paraformaldehyde and stained with DAPI for nuclear labeling. TNT were visualized by staining F actin with phalloidin (488, 594 or 633), after fixation. Cells were permeabilised with 1% of Triton X-100 for 15 min before incubation with phalloidin for 1 h. For live cell imaging, cells were treated with or without rotenone, post transfection with mGFP or mRFP and imaged after 24 h. Mitochondria were visualized in bronchial epithelial cells by confocal microscopy of different lung sections. All images were taken with 63× objective and processed further to clearly visualize mitochondria. For double labeling of mitochondria and bronchial epithelial cells, 5–10 μm lung sections were prepared by cryofrozen microtome and the slides were fixed and processed as described earlier (Ahmad *et al*, 2012). Briefly CCSP (Clara cell secretary protein), which is a specific bronchial epithelial Clara cell marker was used to label bronchial epithelial cells and mitochondria donation from MSC to bronchial epithelial cells were seen as mGFP or mRFP signal, which was co-localized with $CCSP^+$ cells (594 or 643). Alpha smooth muscle actin (α-SMA), a marker of myofibroblasts, was visualized by immunostaining the lung sections with anti-αSMA as described earlier (Ahmad *et al*, 2012). Images were taken with either 10× or 20× objective of a fluorescent microscope (DMI6000).

Immunohistochemistry

Immunohistochemistry for caspase-3, caspase-9 was done as described earlier (Ahmad *et al*, 2011). Antibodies caspase-3 and caspase-9 (Cell Signaling) were used at 1:1,000 dilutions, with overnight incubation at 4°C. Images for immunohistochemistry were taken at 10× or 20× (Nikon Eclipse Ti, Japan).

Fluorescent imaging and live cell microscopy

Live cell microscopy and imaging was done by either live cell fluorescent microscopy (Leica DMI6000, Leica Germany) or confocal microscopy (Leica TCS SP5). Live cell microscopy was done in cells seeded in two or four chamber glass slides (Labtek) under optimal culture conditions, with 37°C of temperature and 5% CO_2. All images showing TNT were captured with either 100× objective (DMI6000) or 63× lambda blue objective (SP5). The images showing the TNT were further processed to show the TNT between the cells. Most of the images showing mitochondria were captured with confocal microscopy. For co-culture experiments epithelial cells were mostly stained with Mitotracker green and MSC or SMC with mito deep red, for 10–20 min in presence of small amounts of probenecid (100 μM) to prevent dye diffusion. The cells were then co-cultured for 24 h. The confocal lasers used for different flourophores with their excitation and emission spectra are given in Table 2.

Table 2. The confocal lasers used for different fluorophores with their excitation and emission spectra

Fluorophores	LASER	Excitation maxima	Emission range
Mitotracker red	DPSS 561	575 nm	580–630 nm
Mitotracker green	ARGON	488 nm	500–540 nm
MitoGFP	ARGON	488 nm	500–540 nm
MitoRFP	DPSS 561	584 nm	580–620 nm
MitoSOX red	ARGON	510 nm	550–650 nm

Confocal imaging was done on Leica TCS SP5 using software LAS AF. Images were acquired by setting proper excitation and emission wavelength using sequential scanning to avoid spillover between spectra.

TUNEL assay

For quantification of apoptosis in different lung cells, lung tissue was dissociated and single-cell suspension were prepared and stained for TUNEL immunofluorescence conjugated with FITC in a similar way as described earlier for IHC (Ahmad *et al*, 2012). Different lung cells were then stained with respective antibodies, such as CCSP (Abcam), for bronchial epithelial cells, SPC (Santa Cruz Biotechnology) for alveolar epithelial cells, alpha smooth muscle actin (Abcam) for mesenchymal cells and F4/80 (Abcam) for macrophages. Respective secondary antibodies conjugated with Alexa Fluor 633 were used. Percentage apoptosis was measured by FACS, by gating on the FL4 window (Alexa Fluor 633) and quantifying the fluorescence on FL1 window (FITC). Dead End Colorimetric TUNEL assay for apoptosis (Promega, USA) was also performed on lung tissue sections using an *in situ* apoptosis detection kit as described earlier (Ahmad *et al*, 2011).

ATP assay

ATP assay was done with Bioluminescence Assay kit (Sigma or Life Technologies, USA) as described earlier for lung tissues (Mabalirajan *et al*, 2008). Same protocol was used for measuring ATP levels in cell lines. ATP levels were measured by using bioluminometer (Berthold AG model) and the total amount of bioluminescent signal was expressed as relative light units (RLU).

Isolation of lung epithelial cells by laser capture microdissection

Bronchial epithelial cells were dissected using laser capture microdissection (LMD Zeiss, Germany). After sacrifice, mice lungs were

cryo-sectioned and cut at 10 μm thickness and slides were fixed with ethanol and stained with methylene blue in order to identify the bronchial epithelium. Around 200 bronchi from each mouse were isolated and total bronchial epithelial cell protein was prepared. Protein estimation was done by BCA method and equal amount of protein was taken for the ELISA assays.

Western blot

Western blotting for Miro1, Miro2, TRAK1, Myo19 and KHC was done as described earlier (21). Total lung protein was prepared and run on 10% polyacrylamide gel. Blots were incubated with primary antibodies [Abcam (USA), Santa Cruz Biotechnology (USA)], at 1:500 dilution & anti-rabbit secondary antibody conjugated with HRP (Sigma) at 1:1,000 dilution.

Histopathology and measurement of airway hyperresponsiveness

Lung histopathology for H&E was done as described earlier (Ahmad *et al*, 2011). Airway resistance (R) was measured using computer controlled invasive airway mechanics measurement instrument, flexivent (Scireq, Canada) as described earlier (Ahmad *et al*, 2011).

ELISA assay

ELISA assay for TGF-β, IL-10 (R&D Biosystems), PGE2 (Cayman), TSLP, IL-25, IL-33 and IDO (USCNK), was done as per the protocols. ELISA assays for different cytokines such as IL-5 (BD Biosciences, USA) and IL-13 (R&D Systems, USA), cytochrome c and mitochondrial complex I and complex IV activity (Sigma Aldrich, USA) was measured as described earlier (Mabalirajan *et al*, 2008; Ahmad *et al*, 2012).

Nitric oxide assay

Nitric oxide was measured in MSC or in their supernatant. Briefly for NO measurement in MSC, cells were labeled with a fluorescent dye, DAF-FM (Life Technologies) and the fluorescence was measured by flow cytometry. For NO measurement in the supernatant, 100 μl of supernatant was taken and measured as per the protocol (Cayman Chemical).

Electron microscopy

Electron microscopy for lung tissues was done as described earlier (Mabalirajan *et al*, 2008).

Statistical analysis

Data are shown as mean ± s.e.m. and is a representative of three experiments, if not mentioned. Statistical significance was set at $P < 0.05$.

Supplementary information for this article is available online: http://emboj.embopress.org

Acknowledgements

Research was supported by grants MLP 5502 and BSC 0403 from the Council of Scientific and Industrial Research, Govt. of India. Anurag Agrawal was supported by DST Swarnjayanti award. We thank Mr. Antony Micheal for helping in doing the live cell experiments and Mr. Mahendra Pratap Singh for helping in electron microscopy. We also thank Drs. Vijay Pal Singh, Naveen Arora and Sanjay Saw for their cooperation in development of the CE allergen induced mice model of AAI. We would also like to acknowledge Dr. Irfan Rahman at University of Rochester, USA for his help. We also acknowledge the help extended by Mudasir Ahmad Malik, Atish Gheware, Vaibhav Jain and Ashish Jaiswal.

Author contributions

The author(s) have made the following declarations about their contributions: TA and SM wrote the paper; conceived, designed and performed the experiments, also analysed the data; BP, MK, BKT, RR, SS, MK, AKJ performed the experiments. APB and MRW provided the human stem cells, SSR, BG and UM analysed the data and wrote the paper, also AA analysed the data, wrote the paper and provided overall scientific guidance and financial support.

Conflict of interest

The authors declare that they have no conflict of interest.

References

Aguilera-Aguirre L, Bacsi A, Saavedra-Molina A, Kurosky A, Sur S, Boldogh I (2009) Mitochondrial dysfunction increases allergic airway inflammation. *J Immunol* 183: 5379 – 5387

Ahmad T, Kumar M, Mabalirajan U, Pattnaik B, Aggarwal S, Singh R, Singh S, Mukerji M, Ghosh B, Agrawal A (2012) Hypoxia response in asthma: differential modulation on inflammation and epithelial injury. *Am J Respir Cell Mol Biol* 47: 1 – 10

Ahmad T, Mabalirajan U, Sharma A, Aich J, Makhija L, Ghosh B, Agrawal A (2011) Simvastatin improves epithelial dysfunction and airway hyperresponsiveness: from asymmetric dimethyl-arginine to asthma. *Am J Respir Cell Mol* 44: 531 – 539

Aich J, Mabalirajan U, Ahmad T, Agrawal A, Ghosh B (2012) Loss-of-function of inositol polyphosphate-4-phosphatase reversibly increases the severity of allergic airway inflammation. *Nat Commun* 3: 877

Brickley K, Stephenson FA (2011) Trafficking kinesin protein (TRAK)-mediated transport of mitochondria in axons of hippocampal neurons. *J Biol Chem* 286: 18079 – 18092

Chang KT, Niescier RF, Min KT (2011) Mitochondrial matrix Ca2+ as an intrinsic signal regulating mitochondrial motility in axons. *Proc Natl Acad Sci USA* 108: 15456 – 15461

Cho YM, Kim JH, Kim M, Park SJ, Koh SH, Ahn HS, Kang GH, Lee JB, Park KS, Lee HK (2012) Mesenchymal stem cells transfer mitochondria to the cells with virtually no mitochondrial function but not with pathogenic mtDNA mutations. *PLoS ONE* 7: e32778

Galluzzi L, Kepp O, Trojel-Hansen C, Kroemer G (2012) Mitochondrial control of cellular life, stress and death. *Circ Res* 111: 1198 – 1207

Gomes LC, Di Benedetto G, Scorrano L (2011) During autophagy mitochondria elongate, are spared from degradation and sustain cell viability. *Nat Cell Biol* 13: 589 – 598

Hase K, Kimura S, Takatsu H, Ohmae M, Kawano S, Kitamura H, Ito M, Watarai H, Hazelett CC, Yeaman C, Ohno H (2009) M-Sec promotes membrane nanotube formation by interacting with Ral and the exocyst complex. *Nat Cell Biol* 11: 1427 – 1432

Islam MN, Das SR, Emin MT, Wei M, Sun L, Westphalen K, Rowlands DJ, Quadri SK, Bhattacharya S, Bhattacharya J (2012) Mitochondrial transfer

from bone-marrow-derived stromal cells to pulmonary alveoli protects against acute lung injury. *Nat Med* 18: 759 – 765

Johnson TM, Yu ZX, Ferrans VJ, Lowenstein RA, Finkel T (1996) Reactive oxygen species are downstream mediators of p53-dependent apoptosis. *Proc Natl Acad Sci USA* 93: 11848 – 11852

Lambrecht BN, Hammad H (2012) The airway epithelium in asthma. *Nat Med* 18: 684 – 692

Liesa M, Palacin M, Zorzano A (2009) Mitochondrial dynamics in mammalian health and disease. *Physiol Rev* 89: 799 – 845

Mabalirajan U, Dinda AK, Kumar S, Roshan R, Gupta P, Sharma SK, Ghosh B (2008) Mitochondrial structural changes and dysfunction are associated with experimental allergic asthma. *J Immunol* 181: 3540 – 3548

Mabalirajan U, Rehman R, Ahmad T, Kumar S, Leishangthem GD, Singh S, Dinda AK, Biswal S, Agrawal A, Ghosh B (2013) 12/15-lipoxygenase expressed in non-epithelial cells causes airway epithelial injury in asthma. *Sci Rep* 3: 1540

Prockop DJ (2012) Mitochondria to the rescue. *Nat Med* 18: 653 – 654

Quintero OA, DiVito MM, Adikes RC, Kortan MB, Case LB, Lier AJ, Panaretos NS, Slater SQ, Rengarajan M, Feliu M, Cheney RE (2009) Human Myo19 is a novel myosin that associates with mitochondria. *Curr Biol* 19: 2008 – 2013

Ren G, Zhang L, Zhao X, Xu G, Zhang Y, Roberts AI, Zhao RC, Shi Y (2008) Mesenchymal stem cell-mediated immunosuppression occurs via concerted action of chemokines and nitric oxide. *Cell Stem Cell* 2: 141 – 150

Rustom A, Saffrich R, Markovic I, Walther P, Gerdes HH (2004) Nanotubular highways for intercellular organelle transport. *Science* 303: 1007 – 1010

Spees JL, Olson SD, Whitney MJ, Prockop DJ (2006) Mitochondrial transfer between cells can rescue aerobic respiration. *Proc Natl Acad Sci USA* 103: 1283 – 1288

Srivastava D, Mehta AK, Arora N, Gaur SN, Singh BP (2010) Proteolytically inactive per a 10 allergen of Periplaneta americana modulates Th2 response and enhances IL-10 in mouse model. *J Clin Immunol* 30: 426 – 434

Swamy M, Jamora C, Havran W, Hayday A (2010) Epithelial decision makers: in search of the 'epimmunome'. *Nat Immunol* 11: 656 – 665

Trian T, Benard G, Begueret H, Rossignol R, Girodet PO, Ghosh D, Ousova O, Vernejoux JM, Marthan R, Tunon-de-Lara JM, Berger P (2007) Bronchial smooth muscle remodeling involves calcium-dependent enhanced mitochondrial biogenesis in asthma. *J Exp Med* 204: 3173 – 3181

Vallabhaneni KC, Haller H, Dumler I (2012) Vascular smooth muscle cells initiate proliferation of mesenchymal stem cells by mitochondrial transfer via tunneling nanotubes. *Stem Cells Dev* 21: 3104 – 3113

Wang X, Veruki ML, Bukoreshtliev NV, Hartveit E, Gerdes HH (2010) Animal cells connected by nanotubes can be electrically coupled through interposed gap-junction channels. *Proc Natl Acad Sci USA* 107: 17194 – 17199

Wang X, Winter D, Ashrafi G, Schlehe J, Wong YL, Selkoe D, Rice S, Steen J, LaVoie MJ, Schwarz TL (2011) PINK1 and Parkin target Miro for phosphorylation and degradation to arrest mitochondrial motility. *Cell* 147: 893 – 906

Yasuda K, Khandare A, Burianovskyy L, Maruyama S, Zhang F, Nasjletti A, Goligorsky MS (2011) Tunneling nanotubes mediate rescue of prematurely senescent endothelial cells by endothelial progenitors: exchange of lysosomal pool. *Aging* 3: 597 – 608

Youle RJ, van der Bliek AM (2012) Mitochondrial fission, fusion, and stress. *Science* 337: 1062 – 1065.

Zhu H, Guo ZK, Jiang XX, Li H, Wang XY, Yao HY, Zhang Y, Mao N (2010) A protocol for isolation and culture of mesenchymal stem cells from mouse compact bone. *Nat Protoc* 5: 550 – 560

